

## Cross-section measurements of nuclides formed by the reaction of 0.20–6.0 GeV protons with $^{197}\text{Au}$

S. B. Kaufman and E. P. Steinberg

*Chemistry Division, Argonne National Laboratory, Argonne, Illinois 60439*

(Received 25 February 1980)

Cross sections of a number of radioactive products formed by the reaction of protons with  $^{197}\text{Au}$  have been measured at bombarding energies of 0.20, 0.49, 1.0, 3.0, and 6.0 GeV. The excitation functions for specific nuclides exhibit several different types of behavior which are characteristic of the reaction mechanisms involved. Spallation products have excitation functions which rise rapidly above an energetic threshold, go through a maximum, and then decrease again, finally approaching a constant cross section at the highest energies. The excitation functions of light nuclides do not exhibit such a peak, but increase monotonically to the asymptotic high-energy limit. Mass-yield distributions are derived from the data, and are compared with the results of intranuclear cascade-evaporation calculations. Comparison of the mass-yield distribution for protons with those for incident pions shows that the rest energy of the pion is as effective in transferring excitation energy to the target as the same amount of kinetic energy.

[NUCLEAR REACTIONS  $^{197}\text{Au}(p, x)$   $^{24}\text{Na}$ – $^{196}\text{Au}$ ,  $E_p = 0.20$ – $6.0$  GeV; measured  $\sigma$ ; derived mass-yield distributions.]

### I. INTRODUCTION

The dependence of the formation cross section of a nuclide upon the bombarding energy of the projectile (the excitation function) has a characteristic shape which often can be related to the reaction mechanism. Such features as the effective energetic threshold, the slope of the excitation function as it rises, and the energy at which it reaches a maximum (if there is a maximum) may all be significant features. Comparisons between different nuclides are useful in pointing up the similarities and differences between their reaction mechanisms. For example, for the reactions of energetic protons with heavy nuclei, one can distinguish between such processes as spallation, fission, and fragmentation, and characterize them by their typical excitation functions.<sup>1</sup>

For a near-spallation product within a few mass numbers of the target, the excitation function rises rapidly above the energetic threshold, goes through a maximum, and then decreases because of the competition from other reactions with higher thresholds. As the mass difference between target and product nuclide increases, the threshold energy and the peak energy also increase, indicating the larger deposition energies required to form the deeper spallation products.

If the target nucleus is easily fissionable, the fission process will compete effectively with spallation in a way which depends on the fission barriers of the various nuclides formed during the deexcitation process. Many light nuclides

are formed by a specifically high-energy process, fragmentation, which is characterized by a rapidly rising excitation function with an apparent threshold in the energy range 0.5–1 GeV.

These qualitative considerations were put on a more quantitative basis by Porile and Sugarman,<sup>2</sup> who analyzed excitation functions to derive a value for the mean deposition energy required to form a specific product nuclide. This analysis requires information on the spectrum of deposition energies given to the target by the incident projectile as a function of the bombarding energy, which was obtained from the results of intranuclear cascade calculations.<sup>3</sup>

At sufficiently high bombarding energies all excitation functions are expected to level off, as formation cross sections become independent of the bombarding energy according to the principle of limiting fragmentation.<sup>4</sup> For protons interacting with heavy targets, such as  $^{197}\text{Au}$  and  $^{238}\text{U}$ , the limiting fragmentation region is attained<sup>5,6</sup> at energies above 10 GeV. This implies that the deposition energy spectrum in the target becomes independent of bombarding energy in that energy regime.<sup>5</sup>

Although the general features of such proton-induced excitation functions are known, there is a surprising lack of experimental data for different targets and product nuclides in the energy range where many cross sections are changing rapidly, i.e., between 0.1 and 3 GeV. The most comprehensive set of data is that of Wolfgang *et al.*,<sup>7</sup> on the interaction of 0.6–3.0-GeV protons with natural Pb. In that work excitation functions

for about 30 nuclides of  $A < 140$  were determined, and the different mechanisms mentioned above could be distinguished. Other studies have focused on a narrow range of product mass numbers, for example, the work of Friedlander *et al.*<sup>8</sup> in which excitation functions for a number of nuclides of  $127 \leq A \leq 140$  formed from 0.1–6.2-GeV protons interacting with uranium were measured. Another example of a complete excitation function is that for  $^{149}\text{Tb}$  formed from 0.6–30-GeV protons interacting with Au, for which the motivation was its use as a beam intensity monitor.<sup>9</sup>

If a sufficient number of nuclide cross sections are measured at a given bombarding energy, a mass-yield curve can be estimated. Knowledge of how such mass-yield curves change with bombarding energy can be of utility in comparing the effects of different projectiles on the same target. For example, a comparison<sup>10</sup> of the mass-yield curves for the reactions of  $\pi^\pm$  mesons and protons with Cu was used to show the importance of pion absorption in depositing excitation energy. Another example is the comparison between protons and relativistic heavy ions, which has been made for several different targets<sup>11–16</sup> in order to study the problem of whether the total energy of the projectile or the energy per nucleon is the important parameter in affecting target fragmentation yields.

The present measurements were carried out in order to provide a set of excitation functions and mass-yield curves for the reactions of protons with Au, and thus facilitate comparisons with other projectiles. As an example, the present data will be compared with published data<sup>17,18</sup> for positive and negative pions interacting with Au.

## II. EXPERIMENTAL PROCEDURE AND RESULTS

The targets consisted of three gold foils, each of  $24 \text{ mg cm}^{-2}$  thickness, of which the central one was used for the radioactivity measurements, being compensated for recoil losses by the adjacent foils.

One bombardment was done at an energy of 200 MeV, using the beam from the AGS injector at Brookhaven National Laboratory. Two bombardments at each of the other energies were done, using the internal beam of the Argonne National Laboratory ZGS accelerator at 1.0, 3.0, and 6.0 GeV, and the external beam of the Intense Pulsed Neutron Generator (IPNS) synchrotron at 490 MeV.

The proton intensity was determined by measuring the amount of  $^{24}\text{Na}$  induced in an aluminum monitor foil of  $7 \text{ mg cm}^{-2}$  thickness, which was similarly guarded by adjacent identical foils.

However, for the 200-MeV experiment no aluminum foils were used, but the production of  $^{196}\text{Au}$  in the target was used as an internal monitor for the proton intensity; its formation cross section at that energy is<sup>19</sup>  $73.6 \pm 6.0 \text{ mb}$ . The values of the  $^{27}\text{Al} \rightarrow ^{24}\text{Na}$  monitor cross sections used at the other bombarding energies were<sup>20</sup> 10.7, 10.5, 9.1, and 8.7 mb, at energies of 0.49, 1.0, 3.0, and 6.0 GeV, respectively.

The target foils were counted using several Ge(Li) spectrometers, and the decay of the  $\gamma$ -ray spectra followed as a function of time. The procedure for the analysis of these spectra and the identification and measurement of individual radio-nuclides has been previously described.<sup>5</sup> Briefly, the GAMANAL<sup>21</sup> program was used to determine the photopeak intensities in the spectra, and the resulting decay curves were extrapolated to obtain the decay rate at the end of the bombardment. From this decay rate, the calibrated photopeak efficiency of the Ge(Li) detector, and the abundance of the observed  $\gamma$  ray in the decay of each nuclide, a cross section could be calculated. The decay properties of the nuclides of interest which were used in this calculation are those listed in our previous work.<sup>5,17</sup>

The cross sections measured in these experiments are given in Table I. The error given with each cross section includes the estimated error in the extrapolated decay rate, obtained from the least-squares decay curve analysis and the statistical uncertainties in photopeak intensities. In addition, a 5% uncertainty in the efficiency calibration of the detectors was folded in. Possible systematic errors in the  $\gamma$ -ray abundances and the monitor cross sections are not included.

As discussed previously,<sup>5,17</sup> the spallation products within 30–40 mass numbers of the target are not the primary products of the reaction, but are largely formed by electron-capture decay of their more neutron-deficient parent nuclides. When the half-life of the observed nuclide is much longer than that of any of its precursors, the cross section may be calculated as if the former were a primary product without significant error. When that is not the case, however, the calculated cross section is too large by a factor of  $\lambda_1 / (\lambda_1 - \lambda_2)$ , where  $\lambda_1$  and  $\lambda_2$  are the decay constants of the parent nuclide and the observed nuclide, respectively. This assumes that the parent is formed entirely as a primary product and the observed nuclide arises entirely by radioactive decay.

The cross sections given in Table I have all been corrected for this effect, with the exception of those nuclides which are shielded from formation in this way, denoted by *I* (independent) in

TABLE I. Formation cross sections of nuclides formed by the reaction of 0.20–6.0 GeV protons with  $^{197}\text{Au}$ . Independent yields are indicated by (I); others are cumulative.

Nuclide	Proton energy (GeV)				
	0.20	0.49	1.0	3.0	6.0
$^{196}\text{Au}$ (I)	73.6 ± 6.0 <sup>a</sup>	70 ± 6	69 ± 6	76 ± 7	73 ± 7
$^{196}\text{Au}^m$ (I)	2.7 ± 0.5	3.2 ± 0.4			
$^{195}\text{Hg}^m$ (I)	9.7 ± 1.0	3.8 ± 0.8			
$^{194}\text{Au}$ (I)	64 ± 5	41 ± 3	32.6 ± 2.5	30.3 ± 2.5	28.8 ± 2.3
$^{193}\text{Hg}^m$ (I)	15.6 ± 1.5	5.9 ± 1.0	2.4 ± 0.3	1.5 ± 0.3	
$^{193}\text{Au}$	103 ± 10	60 ± 8	35 ± 4		
$^{192}\text{Ir}$ (I)	1.22 ± 0.15	2.18 ± 0.22	2.37 ± 0.25	2.13 ± 0.20	2.16 ± 0.20
$^{191}\text{Pt}$	101 ± 9	56 ± 5	38.5 ± 4.0		
$^{190}\text{Ir}$ (I)	2.74 ± 0.25	4.5 ± 0.4	4.3 ± 0.4	3.69 ± 0.35	3.80 ± 0.42
$^{189}\text{Ir}$	85 ± 7	57 ± 4	37.6 ± 3.1		
$^{188}\text{Pt}$	98 ± 7	57 ± 3	33.8 ± 2.5	21.8 ± 1.7	18.9 ± 2.0
$^{188}\text{Ir}$ (I)	6.4 ± 1.3	11.3 ± 1.5	8.6 ± 1.1	6.5 ± 1.0	6.3 ± 1.2
$^{185}\text{Os}$	71 ± 6	70 ± 6	42.2 ± 3.3	26.1 ± 2.2	22.1 ± 2.3
$^{183}\text{Re}$	33.5 ± 2.9	60 ± 5	37.0 ± 3.1	20.7 ± 1.8	17.7 ± 2.1
$^{182}\text{Os}$	24.1 ± 2.2	55 ± 5	35.8 ± 3.4	22.5 ± 3.0	
$^{181}\text{Re}$	19.7 ± 1.8	60 ± 5	39.9 ± 3.1	22.4 ± 2.1	17.7 ± 2.5
$^{175}\text{Hf}$	0.52 ± 0.06	35.9 ± 2.5	41.3 ± 2.8	21.7 ± 1.9	17.2 ± 1.6
$^{173}\text{Lu}$		31.2 ± 2.7	47.9 ± 3.6	25.4 ± 2.3	19.8 ± 2.0
$^{172}\text{Hf}$		23.1 ± 2.0	37.0 ± 2.8	18.8 ± 1.5	14.7 ± 1.6
$^{171}\text{Lu}$		20.6 ± 1.6	40.1 ± 2.7	20.6 ± 1.5	15.7 ± 1.3
$^{170}\text{Lu}$		15.7 ± 1.5	32.9 ± 2.6	17.3 ± 1.5	13.3 ± 1.2
$^{167}\text{Tm}$		9.6 ± 0.7	32.0 ± 2.5	18.2 ± 1.7	14.0 ± 1.3
$^{149}\text{Gd}$			11.4 ± 1.2	22.0 ± 2.0	15.4 ± 1.4
$^{146}\text{Gd}$			6.8 ± 0.6	17.3 ± 1.5	12.3 ± 1.0
$^{145}\text{Eu}$			5.9 ± 0.6	18.5 ± 1.7	13.8 ± 1.2
$^{139}\text{Ce}$			1.90 ± 0.24	12.8 ± 1.4	9.6 ± 1.0
$^{134}\text{Ba}$			1.4 ± 0.3	11.4 ± 1.3	8.4 ± 1.0
$^{127}\text{Xe}$			0.88 ± 0.12	10.4 ± 0.9	8.6 ± 0.9
$^{124}\text{Te}$			0.50 ± 0.10	6.9 ± 0.8	6.0 ± 0.7
$^{105}\text{Ag}$				3.5 ± 0.4	4.0 ± 0.5
$^{103}\text{Ru}$	0.96 ± 0.11	1.04 ± 0.14	0.72 ± 0.09	0.37 ± 0.06	0.41 ± 0.05
$^{96}\text{Tc}$ (I)			0.86 ± 0.10	2.00 ± 0.18	2.44 ± 0.22
$^{95}\text{Nb}$ (I)	0.79 ± 0.11	1.42 ± 0.17	1.03 ± 0.10	0.82 ± 0.08	0.75 ± 0.10
$^{95}\text{Zr}$	0.48 ± 0.10	0.55 ± 0.11	0.44 ± 0.06	0.26 ± 0.05	0.26 ± 0.05
$^{90}\text{Nb}$			0.93 ± 0.12	3.18 ± 0.25	4.17 ± 0.40
$^{89}\text{Zr}$	0.14 ± 0.05	0.94 ± 0.12	1.53 ± 0.12	3.89 ± 0.30	5.17 ± 0.37
$^{87}\text{Y}$	0.23 ± 0.06	1.10 ± 0.13	1.90 ± 0.21	4.78 ± 0.35	6.22 ± 0.55
$^{84}\text{Rb}$ (I)		1.11 ± 0.20	1.44 ± 0.25	1.44 ± 0.30	1.60 ± 0.35
$^{83}\text{Rb}$		1.49 ± 0.18	2.50 ± 0.23	4.47 ± 0.35	6.2 ± 0.6
$^{75}\text{Se}$		0.53 ± 0.10	1.35 ± 0.14	2.96 ± 0.30	4.33 ± 0.40
$^{74}\text{As}$ (I)		0.83 ± 0.09	1.38 ± 0.13	1.98 ± 0.20	2.26 ± 0.25
$^{65}\text{Zn}$		0.22 ± 0.03	0.71 ± 0.08	2.00 ± 0.18	3.08 ± 0.25
$^{59}\text{Fe}$		0.36 ± 0.04	0.62 ± 0.06	1.14 ± 0.10	1.41 ± 0.15
$^{58}\text{Co}$ (I)			0.41 ± 0.06	1.55 ± 0.16	2.78 ± 0.35
$^{54}\text{Mn}$ (I)		0.12 ± 0.03	0.44 ± 0.04	1.95 ± 0.20	3.31 ± 0.35
$^{52}\text{Mn}$ (I)				0.61 ± 0.10	0.99 ± 0.12
$^{48}\text{V}$				0.58 ± 0.07	1.15 ± 0.15
$^{46}\text{Sc}$ (I)			0.38 ± 0.05	2.19 ± 0.20	3.60 ± 0.32
$^{28}\text{Mg}$				1.31 ± 0.14	2.44 ± 0.22
$^{24}\text{Na}$			0.53 ± 0.06	5.7 ± 0.5	10.3 ± 1.3

<sup>a</sup>Monitor cross section, Ref. 19.

Table I. This correction is < 5% for all nuclides listed, except for the following three, for which  $\lambda_1/(\lambda_1 - \lambda_2)$  is given in parentheses:  $^{170}\text{Lu}$ (1.454),  $^{181}\text{Re}$ (1.096), and  $^{171}\text{Lu}$ (1.066).

For several nuclides, the present measurements can be compared to previous results<sup>22-29</sup> at the same or similar bombarding energies. The agreement, in general, is satisfactory; these

previous measurements are shown as additional data points on the excitation functions in the following section (Figs. 1-4).

### III. DISCUSSION

#### A. Excitation functions

The excitation functions for the various nuclides measured here exhibit trends which vary in a regular way with nuclide mass number. For the medium-mass nuclides ( $50 \leq A \leq 110$ ), there are differences between neutron-excess and neutron-deficient nuclides as well. The differences in excitation functions are correlated with different reaction mechanisms; indeed, the excitation function is one of the ways different reaction mechanisms are characterized. Thus it is convenient to group the product nuclides into spallation, fission, and fragmentation products, using their excitation functions to classify them.

The nuclides whose excitation functions are shown in Fig. 1 are representative of those whose mass numbers are close to the target, the near-spallation products. Figure 1(a) shows the excitation functions for  $^{196}\text{Au}$  and  $^{194}\text{Au}$  as examples of the simplest spallation reactions, including data in the literature<sup>19</sup> for  $^{196}\text{Au}$ . It is seen that the cross section for the simple reaction  $^{197}\text{Au}(p,pn)^{196}\text{Au}$  is essentially constant above an energy of 0.2 GeV. This is a well-known<sup>30</sup> characteristic of  $(p,pn)$  reactions in general, and pro-

bably is a result of the peripheral nature of such reactions, involving small energy transfer. They may occur either by a quasi-free scattering in which both nucleons escape the nucleus, or by an inelastic scattering which excites the nucleus enough to permit evaporation of only one neutron.<sup>30</sup> There is evidence<sup>31</sup> that at 400 MeV both these processes contribute about equally for an  $^{197}\text{Au}$  target. At lower bombarding energies than shown in Fig. 1(a) the  $(p,pn)$  cross section goes through a broad maximum,<sup>32</sup> reaching a value of about 180 mb at 45 MeV.

The cross section for  $^{194}\text{Au}$  also has a peak<sup>32</sup> at lower energies than shown in Fig. 1(a), and the decrease from this peak with increasing energy is shown by the present data. The  $^{194}\text{Au}$  excitation function is seen to decrease until it also becomes constant above an energy of a few GeV. The pattern seen for these two nuclides is quite general; any product from the reaction of a charged particle with a nucleus must have an initially rising excitation function, due to energetic and Coulomb barrier thresholds. At the high-energy limit, on the other hand, all cross sections appear to reach asymptotic values.<sup>5</sup> It is the behavior between these limits which differs for various products: the presence of a peak (or several peaks)<sup>33</sup> and the peak energy, or else a monotonic rise to the asymptotic cross section.

Cross sections for the formation of the high spin ( $12^-$ ) isomeric state  $^{196}\text{Au}^m$  were determined only at bombarding energies of 200 and 490 MeV, because at higher energies the greatly increased complexity of the  $\gamma$ -ray spectra obscured the isomeric transition. However, at those two energies the isomeric ratio  $\sigma(12^-)/\sigma(2^-)$  is quite small,  $\sim 0.04$ , which is indicative of the small amount of angular momentum imparted by the simple  $(p,pn)$  reaction.

Isomeric states of two isotopes of Hg were also observed,  $^{195}\text{Hg}^m$  at the two lowest energies and  $^{193}\text{Hg}^m$  up to 3 GeV. Although their excitation functions are not shown graphically, it can be seen from the data in Table I that their cross sections decrease rapidly with increasing energy; the energy dependence below 1 GeV is approximately inverse in bombarding energy. This behavior has been previously observed<sup>34-36</sup> in  $(p,xn)$  excitation functions; the energy dependence is similar to that of the free-particle  $p$ - $n$  scattering cross section in the same energy region. This suggests that the primary mechanism for  $(p,xn)$  reactions is a quasifree  $p$ - $n$  charge-exchange scattering, resulting in an excited nucleus which subsequently may evaporate one or more neutrons.

Figure 1(b) shows the excitation functions for two

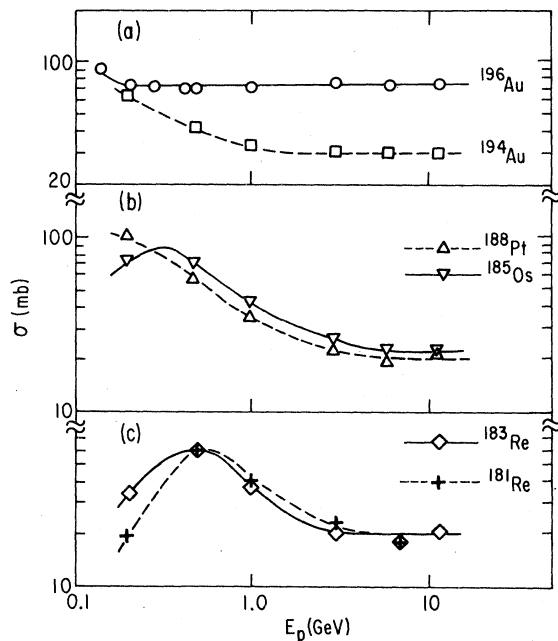


FIG. 1. Excitation functions for representative spallation products of the interaction of protons with  $^{197}\text{Au}$ .

spallation products somewhat further from the target,  $^{188}\text{Pt}$  and  $^{185}\text{Os}$ . The cross section of  $^{188}\text{Pt}$  decreases from 200 MeV to 6 GeV, above which energy it is constant. The peak in the excitation function must occur below 200 MeV. However, it is likely that the excitation function for  $^{185}\text{Os}$  peaks above 200 MeV, since the cross sections at 200 and 490 MeV are equal; the smooth curve for  $^{185}\text{Os}$  has been drawn to show such a peak.

The cross sections for  $^{183}\text{Re}$  and  $^{181}\text{Re}$  [Fig. 1(c)] definitely indicate a peak in the vicinity of 0.5 GeV, with the lighter isotope probably peaking at a higher energy. The general trend with increasing mass loss from the target is for the energy of the peak to increase and the maximum cross section to decrease. Moreover, the bombarding energy above which the cross section is constant also increases with the mass loss.

These trends are evident in the excitation functions for deeper spallation products with  $\Delta A > 20$ , as shown in Fig. 2. Since the present measurements are at rather widely spaced energies where the cross sections are changing rapidly, it was helpful in drawing the smooth curves in Fig. 2 to use the well-determined<sup>9</sup> excitation function for  $^{149}\text{Tb}$  as a guide. The latter data are for the  $\alpha$ -decay branch, and have been scaled by a factor of 10 for convenience of display. Measurements of the  $^{127}\text{Xe}$  cross section<sup>22</sup> at 3 and 28 GeV have been included in Fig. 2.

The initial rise in cross section is quite steep

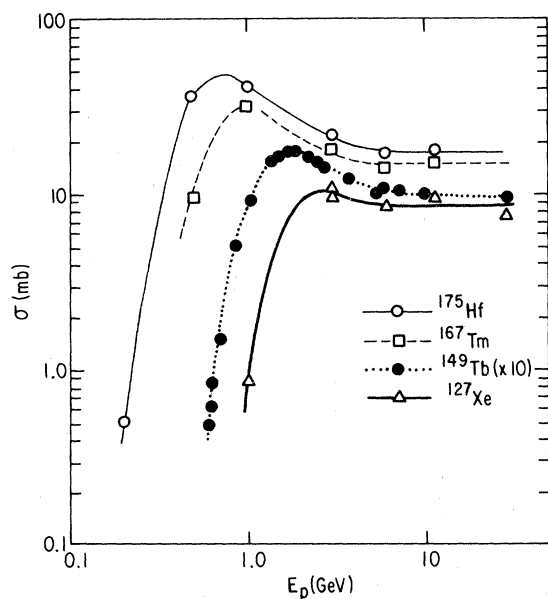


FIG. 2. Excitation functions for representative deep spallation products. The data for  $^{149}\text{Tb}$  are from Ref. 9 and are for the  $\alpha$ -decay branch; it is scaled up by a factor of 10 for convenience of comparison.

for these nuclides, indicating the importance of high deposition energies in their formation. Again one sees the energy at which the excitation function peaks increasing with distance from the target, and the peak cross section decreasing. The asymptotic value at high energy also decreases, but not as rapidly. This has the effect that the peak becomes less prominent, and for  $^{127}\text{Xe}$ , with  $\Delta A = 70$ , the peak is only suggested.

The picture becomes less clear for still lighter nuclides, because of the varying contributions of deep spallation, fission, and fragmentation. In Fig. 3 are shown the excitation functions for some light nuclides,  $^{24}\text{Na}$ ,  $^{28}\text{Mg}$ , and  $^{46}\text{Sc}$ , which are generally termed fragmentation products. The nuclide  $^{87}\text{Y}$  is also included in this figure, as a typical example of a medium-mass, neutron-deficient product, since it has a somewhat similar excitation function to the lighter nuclides. Data from the literature<sup>25-29</sup> are included for  $^{24}\text{Na}$ ,  $^{28}\text{Mg}$ , and  $^{46}\text{Sc}$ . Although these products share with the deep spallation products the sharply rising excitation function, they do not exhibit the peak and subsequent falloff of the latter. Instead one sees a monotonic increase to the asymptotic value; the flattening of the cross sections does not occur until an energy of approximately 10 GeV.

The excitation function of  $^{87}\text{Y}$  differs from those of the lighter nuclides in its less steep slope; this is a consequence of a changing contribution

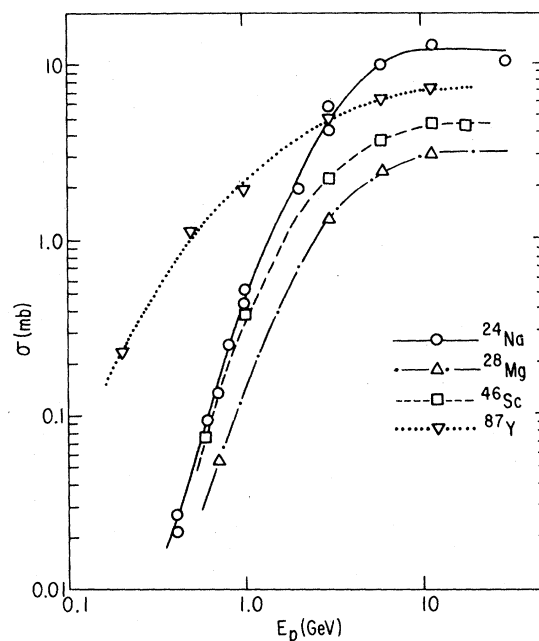


FIG. 3. Excitation functions for typical light fragmentation products.

of different mechanisms with bombarding energy. At 200 MeV, nuclides such as  $^{87}\text{Y}$  and  $^{89}\text{Zr}$  are formed by a binary fission mechanism; they lie on the neutron-deficient wing of the charge-dispersion curve, and their cross sections are smaller than those of the neutron-excess fission products, such as  $^{103}\text{Ru}$ . With increasing bombarding energy the contribution of fragmentation and deep spallation to the formation of the neutron-deficient, medium-mass nuclides increases. This change is also revealed in the change in recoil properties of these nuclides: The mean kinetic energies of these nuclides, as derived from their recoil ranges, decrease by about a factor of 2 as the bombarding energy increases.<sup>37</sup> The fission process results in a higher kinetic energy than do the other mechanisms, and thus the changing mechanisms are revealed by the mean recoil kinetic energy. In contrast, the mean kinetic energy of light nuclides, such as  $^{24}\text{Na}$ , is nearly independent of proton bombarding energy,<sup>37</sup> indicating no fundamental change in reaction mechanism.

Figure 4 shows the excitation functions for other medium-mass nuclides, which further illustrate these effects of the different mechanisms. In Fig. 4(a) are shown excitation functions for some medium-mass nuclides which are near the line of beta stability, and whose excitation functions rise with increasing energy, but not as steeply as that of the neutron-deficient  $^{87}\text{Y}$ . Thus one concludes that the high-energy mechanisms of deep spallation or fragmentation make less of a contribution to such nuclides at high energy than

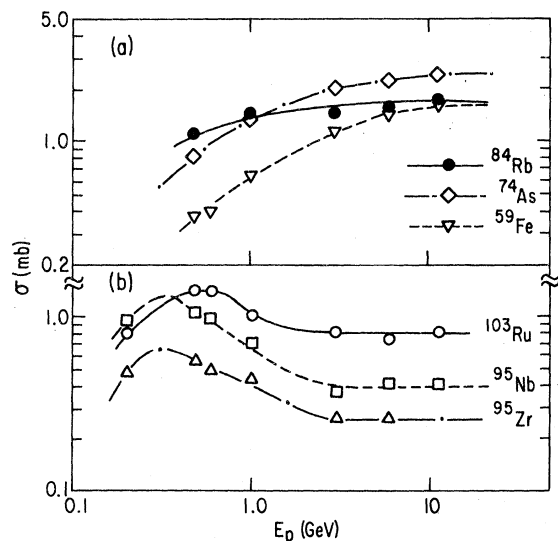


FIG. 4. Excitation functions for representative medium-mass products.

to more neutron-deficient nuclides.

In contrast to these rising excitation functions are those for the more neutron-excess nuclides shown in Fig. 4(b), which peak at energies of 300–500 MeV and then fall off before reaching the usual asymptotic behavior at high energies. These nuclides are probably formed almost entirely by binary fission, and their excitation functions are similar to that for fission, as measured by track detectors.<sup>38</sup>

Although the excitation functions for each individual nuclide could be analyzed in the way outlined by Porile and Sugarman,<sup>2</sup> using the results of intranuclear cascade calculations to derive the mean deposition energies required to form that nuclide, it seems preferable to compare the data directly with the results of a cascade-evaporation calculation. This is done in the following section, in which mass-yield distributions are estimated at each bombarding energy.

#### B. Mass-yield curves

The estimation of a mass-yield curve from measurements of formation cross sections for the case of a heavy target such as gold has been previously discussed.<sup>5,17</sup> For nuclides in the spallation region (i.e.,  $\Delta A \lesssim 70$ ) the primary nuclides tend to be highly neutron-deficient relative to the valley of beta stability because of the preponderance of deexcitation by neutron evaporation. Therefore, the radionuclides observed in the present work are formed mainly by the electron-capture decay of the primary products, and their cumulative cross sections measure the major part of the total isobaric cross section at each mass number.

There are two mass regions which are exceptions to this behavior: nuclides near the target and nuclides near the  $N=82$  neutron shell. Close to the target, substantial cross sections for stable nuclides are possible, and thus the observed yields for nuclides such as  $^{196}\text{Au}$  and  $^{194}\text{Au}$  represent only a part of the total isobaric yield. Just above the  $N=82$  shell many nuclides have an appreciable branching ratio for  $\alpha$  decay; this depletes the yield at one mass number and correspondingly enhances it at the mass number four units smaller. Three nuclides listed in Table I have enhanced cross sections due to  $\alpha$  decay of heavier nuclides:  $^{149}\text{Gd}$ ,  $^{146}\text{Gd}$ , and  $^{145}\text{Eu}$ . Correcting the data for this effect was not attempted because of lack of knowledge of the charge dispersion curve, i.e., the variation of primary yield with  $Z$  at constant  $A$ . For this reason it is expected that the cross sections for these three nuclides may fall above the smooth mass-yield

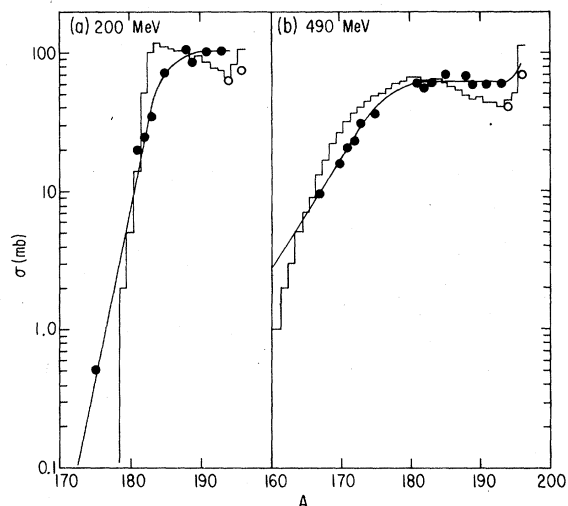


FIG. 5. Mass-yield distributions at energies of 200 and 490 MeV. Solid points are cumulative cross sections, open points are independent. The smooth curves are the estimated experimental mass-yield distributions. The histograms are the results of an intranuclear cascade-evaporation calculation.

curve.

The formation cross sections as a function of mass number for the near-spallation region ( $\Delta A \lesssim 30$ ) are shown in Fig. 5 for proton energies of 200 and 490 MeV. The open symbols are used for  $^{194}\text{Au}$  and  $^{196}\text{Au}$  to indicate that the independent cross sections for these nuclides do not represent the total isobaric cross section at those mass numbers. The smooth curves in Fig. 5 are drawn to show that general trend of the variation of isobaric cross section with mass number. Within a variation of about 20% it is evident that there is indeed such a smooth dependence; close to the target the isobaric cross sections appear to be essentially constant, forming a plateau whose length is greater at the higher bombarding energy. Further from the target the cross sections begin to decrease and exhibit an approximately exponential dependence on  $\Delta A$  at large  $\Delta A$ , with a slope which becomes less steep at the higher bombarding energy.

The exponential dependence on  $\Delta A$  is a feature of spallation cross sections which is well known and has been used in semiempirical equations proposed<sup>39,40</sup> for the estimation of these cross sections. There is no provision, however, in these equations for the plateau observed in the present data. The reason is that the equations were based on spallation cross sections of elements much lighter than gold ( $A \lesssim 100$ ); there have been no adequate measurements of such near-spallation products for a heavy (but rela-

tively nonfissionable) target prior to the present ones.

It is of interest to compare the experimental cross sections with the results of an intranuclear cascade-evaporation calculation to see to what extent the latter can reproduce the observed shape of the mass-yield curve. For this purpose, the VEGAS-ISOBAR intranuclear cascade calculation<sup>41-43</sup> was run for the specific proton energies used in this work; the evaporation stage was treated using the formalism of Dostrovsky, Fraenkel, and Friedlander.<sup>44</sup> The results are shown by the histograms in Fig. 5.

Qualitatively, the agreement between the calculation and the experimental data is fairly good. There is a region near the target where the cross sections are large and do not change much with increasing mass loss, which corresponds approximately to the experimental plateau. For larger mass losses the calculated cross sections decrease in an approximate exponential manner, also in agreement with experiment, both as to slope and to the mass number at which the decrease begins. The main feature of the calculation which does not appear to be supported by the data is the local minimum near  $A = 192-194$ . In addition, at 200 MeV the break between the plateau and the exponential decrease is more abrupt in the calculation than appears to be the case experimentally.

The deexcitation step of the calculation considers only evaporation of nucleons and light nuclei (up to  $^4\text{He}$ ), but does not include fission. The binary fission cross section for  $^{197}\text{Au}$  bombarded with protons is about 35 mb at 200 MeV and 60 mb at 490 MeV,<sup>38</sup> so that the neglect of fission in the calculation does not distort the spallation cross sections appreciably. Although some cross sections for fission products were measured at these energies in the present work, there are too few to permit the estimation of the mass-yield curve for fission. However, a large number of fission products were measured by Kruger and Sugarman<sup>45</sup> at a proton energy of 450 MeV, and they were able to estimate the mass-yield curve.

Figure 6 shows the cross sections as a function of mass number at 1.0 GeV; in addition, the fission mass-yield curve at 0.45 GeV taken from Kruger and Sugarman<sup>45</sup> is shown as the dotted curve for comparison. In the spallation region, as at lower energies, the cumulative cross sections of neutron-deficient nuclides are a good estimate of the total isobaric cross sections; these are shown as the solid points in Fig. 6. The full line indicates the best estimate of the dependence of total isobaric cross section on mass number for  $121 \leq A \leq 197$ ; it has a constant value

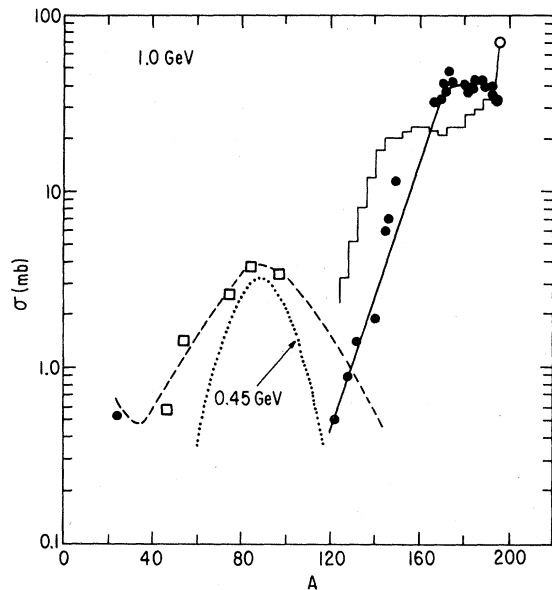


FIG. 6. Mass-yield distribution at 1.0 GeV. Solid points are cumulative cross sections, open squares indicate estimated total isobaric cross sections (see text). Solid curve is the experimental spallation distribution, dashed curve the fission distribution. The fission distribution at 0.45 GeV (dotted curve) is from Ref. 45. Histogram is the result of a cascade-evaporation calculation.

of 40 mb for  $171 \leq A \leq 195$  and decreases exponentially for  $A < 170$ . As discussed above, near  $A = 146$  the experimental data are higher than the curve because of feeding by  $\alpha$  decay.

In the mass range  $24 \leq A \leq 103$ , both neutron-excess and neutron-deficient nuclides are formed with appreciable cross sections. It is necessary to estimate the charge-dispersion curve (i.e., the variation of cross section with  $Z$  at constant  $A$ ) in order to calculate the isobaric cross section. In previous work<sup>5</sup> at 11.5 GeV the charge dispersion curves were obtained as the function<sup>39</sup>

$$\sigma(Z, A) = \sigma(A) \exp(-R|Z - SA + TA^2|^{3/2}), \quad (1)$$

and the parameters  $R$ ,  $S$ , and  $T$  were fitted to the data, both in the spallation mass region and in the medium to light mass range. Using this function to fit the data at 1.0 GeV, it was found that the values of  $R$  and  $S$  used at 11.5 GeV were unchanged, but the parameter  $T$  was larger. This means that the width of the charge dispersion curve at a given mass number is the same at the two energies, but the most probable charge is smaller at the lower energy (i.e., the peak is more neutron excessive). The values of these parameters for the 1.0-GeV data are

$$\begin{aligned} R &= 30A^{-0.79}, \\ S &= 0.470, \\ T &= 3.2 \times 10^{-4}. \end{aligned} \quad (2)$$

Using these values and the expression (1) the total isobaric cross section was calculated for the mass numbers  $A = 46, 54, 74, 84$ , and  $96$ , by fitting the experimental data to obtain  $\sigma(A)$ .

These cross sections are shown as the open squares in Fig. 6; the dashed curve then was drawn to represent the mass-yield curve in the "fission" mass region by using the curve at 0.45 GeV as a guide. At the higher energy the width of the curve is greater and the peak cross section is also larger. These changes are primarily due to the rapidly rising excitation functions for the light fragments and neutron-deficient medium mass nuclides (Fig. 3), since the cross sections for the neutron-excess fission products [Fig. 4(b)] actually decrease somewhat in this energy interval. In the mass region  $120 \leq A \leq 130$  there is an overlap between fission and deep spallation, as indicated by the respective curves crossing.

The histogram in Fig. 6 represents the results of the cascade-evaporation calculation for 1.0-GeV protons. The discrepancies between the calculated and experimental cross sections are clear from this comparison: The calculated cross sections decrease with decreasing  $A$ , instead of being nearly constant for  $175 \leq A \leq 195$ , and a plateau appears for  $145 \leq A \leq 175$ , where the experimental cross sections decrease rapidly. For still smaller mass numbers, the calculated distribution remains above the experimental one. In terms of the spectrum of deposition energies imparted by the cascade, the calculation fails to predict enough low-energy events and over-predicts high-energy ones. However, it must be recognized that at least some of the highest deposition energy cascades should result in fragmentation products rather than simply lead to a long evaporation chain. If the fragmentation mechanism were to be included in some way, this would lower the calculated curve for  $A \leq 160$ , and result in better agreement with experiment.

The mass-yield curves at 3.0 and 6.0 GeV are shown in Figs. 7(a) and 7(b), respectively. At 3.0 GeV there exist data in the literature<sup>22, 24</sup> on total isobaric cross sections at specific mass numbers, and these data are indicated in Fig. 7(a) by the open triangles. The open squares show the total isobaric cross sections estimated from the present data by using the empirical charge dispersion equation [Eq. (1)], with the same values of  $R$  and  $S$  used at 1.0 GeV [Eq. (2)], and a value of  $T = 2.6 \times 10^{-4}$ , which reflects the shift

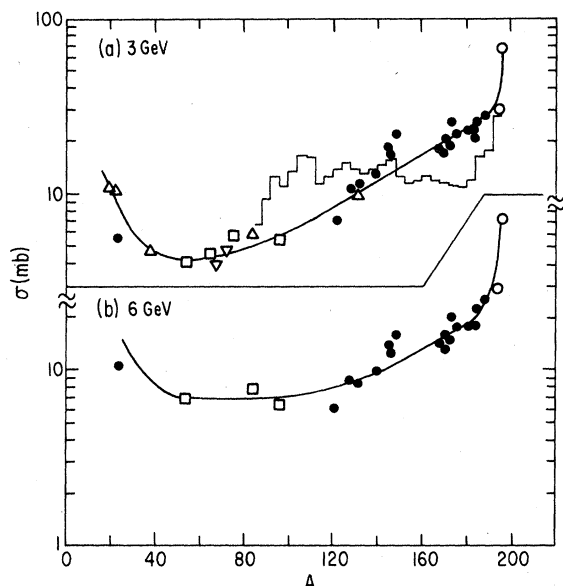


FIG. 7. Mass-yield distributions at energies of 3.0 and 6.0 GeV. See text for explanation of symbols. Histogram is the result of a cascade-evaporation calculation.

in the most probable charge at a given mass number to a larger value (more neutron deficient) than at 1.0 GeV. The filled data points show the cumulative cross sections in the spallation region, and also that for  $^{24}\text{Na}$ . The smooth curve in Fig. 7(a) shows the estimated mass-yield curve based on the experimental data, while the histogram shows the results of the intranuclear cascade-evaporation calculation, where the cascade program of Bertini<sup>46</sup> was used, since the VEGAS-ISOBAR program<sup>41-43</sup> is valid only up to 1.0 GeV.

The experimental mass-yield curve at 3.0 GeV is quite different in shape from that at 1.0 GeV and below. The distinct fission peak which is a prominent feature at the lower energies has disappeared at 3.0 GeV because of the rapidly increasing cross sections of the deep spallation products and the light fragmentation products on either side. Instead of a separate fission peak at  $A \approx 90$  there is only a broad minimum at  $A \approx 50$ . Another change at the higher energy is that the cross section plateau close to the target has changed to a monotonic decrease of cross section with decreasing mass number.

The cascade-evaporation calculation at 3.0 GeV bears no resemblance to the experimental data. There is a rapid decrease in cross section with increasing mass loss from the target, and then there is a nearly constant (ignoring the statistical fluctuations of the calculation) cross section over a broad mass range, down to  $A \approx 100$ . As dis-

cussed above, the calculation is probably unrealistic for the highest deposition energies, since one expects specifically high-energy mechanisms such as fragmentation to occur rather than a long statistical evaporation chain. Thus the part of the calculated mass-yield curve below  $A \approx 150$ , which lies above the experimental curve, would be lowered if such a fragmentation mechanism were included in the calculation.

However, the cascade calculation also predicts a considerably smaller probability for the relatively near-spallation products than is observed, i.e., it underestimates the probability of small deposition energies. Previous comparisons<sup>46</sup> between the results of this intranuclear cascade calculation at 3 GeV and experimental data on spallation of arsenic<sup>47</sup> and silver<sup>48</sup> showed reasonably good agreement, in contrast to the poor agreement found here for the spallation of gold. It may be the case that there are deficiencies in the model which only become apparent for heavy target nuclei, and which result in the underestimation of the probability of low deposition energies.

The mass-yield curve at 6.0 GeV, as shown in Fig. 7(b), is more uncertain than at 3.0 GeV in the middle mass region because of fewer mass numbers at which the total isobaric cross section could be estimated (shown by the open squares). The main change is the higher cross sections for  $A \leq 100$ ; this is also clearly shown in the excitation functions (Fig. 3). There appears to be little further change in cross sections above 6.0 GeV, as shown by the approach to a constant value of the excitation functions (Figs. 1-4) above that energy.

The changes in the mass-yield curve for gold as the proton energy increases from 0.20 to 11.5 GeV are depicted in Fig. 8, in which the smooth mass-yield curves at the different energies are all shown for comparison. In Fig. 8 one can see how the prominent fission peak at low energies broadens and then gets washed out by the rapidly increasing fragmentation and deep spallation cross sections. The changes in the near-spallation region are also evident, with the plateau of constant cross sections lengthening with increasing energy up to 1.0 GeV, and then disappearing at 3.0 GeV.

These qualitative changes in the mass-yield curve for heavy targets with increasing bombarding energy have been pointed out previously in the literature. Wolfgang *et al.*<sup>7</sup> showed similar curves in comparing their data for a Pb target bombarded with 3-GeV protons with Pb and Bi targets at energies of 340 and 480 MeV. Grover<sup>49</sup> compared data for Ta bombarded with 5.7-GeV protons with previous measurements at 340 and

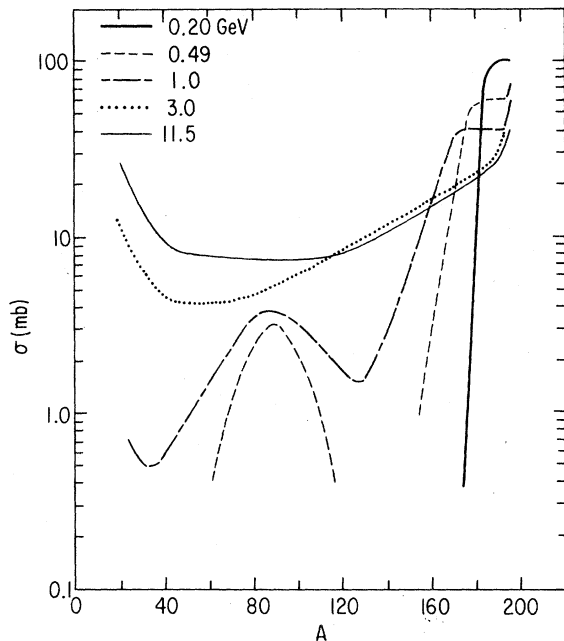


FIG. 8. Comparison of the mass-yield distributions for protons of energies 0.20–11.5 GeV interacting with  $^{197}\text{Au}$ .

450 MeV and showed the same trends. The present work provides data for such systems at more bombarding energies, so that the changes are shown in more detail. Thus, it appears from Fig. 8 that the most significant qualitative change in the mass-yield curve is between 1.0 and 3.0 GeV.

There is evidence from recoil studies on heavy targets that indicates a qualitative change in reaction mechanism in this same energy region. At about 3-GeV incident energy the forward-to-backward ratio, as measured in thick-target, thick-catcher experiments, of many deep spallation and fragmentation products goes through a maximum.<sup>37, 50-53</sup> In addition, the mean kinetic energies of many of these products decrease significantly between 1.0 and 3.0-GeV incident energy. The decrease in forward peaking has been confirmed by measurements of angular distributions using thin targets<sup>54-56</sup> and is associated with a change to sideward peaking in the laboratory system. Thus, a variety of experimental data point to a new, high-energy reaction mechanism of protons which becomes prominent between bombarding energies of 1 and 3 GeV.

Although measurements of formation cross sections and comparisons of the mass-yield curves derived from them are certainly less sensitive indicators of changes in nuclear reaction mechanisms than are the kinematic mea-

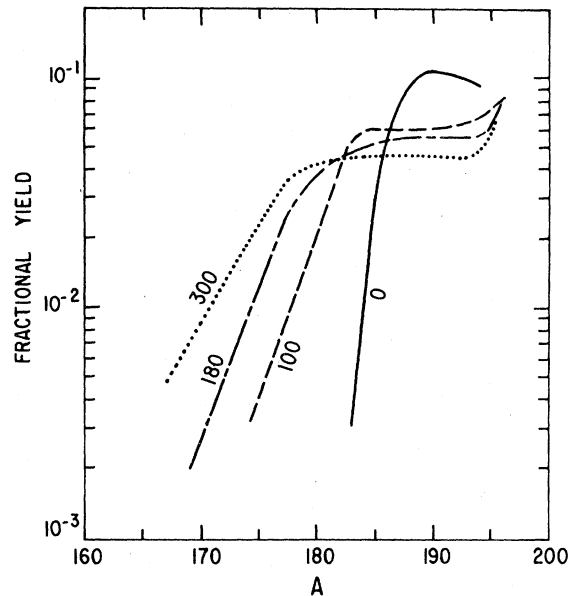


FIG. 9. Mass-yield distributions for  $\pi^-$  mesons of energies 0–300 MeV interacting with  $^{197}\text{Au}$  (from Ref. 17).

surements such as energy and angular distributions, they are useful when the available beam intensities for certain projectiles are so low that the latter experiments are difficult or impractical. This is currently the case for pi mesons and for relativistic heavy ions, for which projectiles some comparisons of mass-yield curves have recently been made.<sup>10-16</sup>

We have previously<sup>17</sup> measured spallation cross sections for positive and negative pions between 100 and 300 MeV reacting with Au, and estimated mass-yield curves from those data. It was found that the shapes of the curves for positive and negative mesons were the same, only differing in magnitude and that the difference appeared due entirely to the difference in Coulombic repulsion (attraction) of positive (negative) pions by the nucleus. Figure 9 shows the mass-yield curves, in terms of fractional yield, relative to the total reaction cross section, for the three pion energies studied. The curve for stopped negative pions<sup>18</sup> is also shown in Fig. 9.

Qualitatively these curves for pions are similar to those shown in Figs. 5 and 6 for protons up to 1 GeV. For both types of projectiles there is a plateau of nearly constant cross section which begins a few mass numbers below the target, whose length increases with increasing bombarding energy. At larger mass differences from the target, cross sections fall off exponentially, with a slope which decreases with increasing bombarding energy.

A simple parameter to characterize the mean

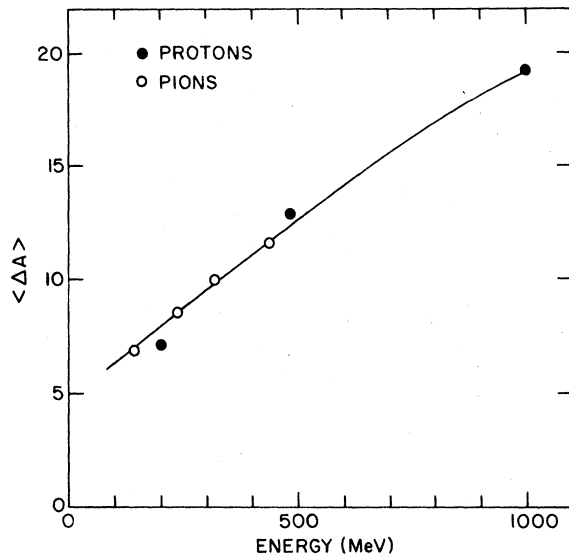


FIG. 10. Average mass lost from the target  $\langle \Delta A \rangle$  as a function of kinetic energy for protons (solid points) and of total energy for pions (open points).

excitation energy for a particular projectile-target system is the average mass lost from the target,  $\langle \Delta A \rangle$ . From the systematics of the cascade-evaporation calculations<sup>41-44</sup> it can be estimated that about 10 MeV of excitation energy is required, on the average, for each nucleon lost. Since this applies only to evaporation residues, one should include only that portion of the mass-yield curve in calculating  $\langle \Delta A \rangle$ . Clearly, the fission mechanism achieves a large mass loss for

a relatively small amount of excitation energy, and thus the fission mass region should not be included. Such a distinction is only possible up to 1.0 GeV, since there is no clear separation of different mechanisms at the higher energies (Fig. 7).

We have calculated values for  $\langle \Delta A \rangle$  from the smooth mass-yield curves in the spallation region for proton energies up to 1.0 GeV, and they are shown in Fig. 10 as a function of bombarding energy. For comparison the same quantity for incident pions<sup>17</sup> is also plotted at an energy equal to the sum of the rest mass energy of the pion and its kinetic energy. These data show that the mean excitation energy imparted to the nucleus, as measured by the mean mass lost, is comparable for protons of a given kinetic energy and pions of about 140 MeV lower kinetic energy. The rest energy of the pion is thus about as effective in transferring energy to a heavy nucleus as is the projectile kinetic energy.

#### ACKNOWLEDGMENTS

We wish to thank Dr. P. E. Haustein for carrying out the 200-MeV bombardment at Brookhaven National Laboratory and shipping us the target. The cooperation and assistance of the ZGS operating staff was essential for the bombardments at the higher energies. This research was performed under the auspices of the Office of Basic Energy Sciences, Division of Nuclear Physics, U. S. Department of Energy.

<sup>1</sup>For a review, see J. Hudis, in *Nuclear Chemistry*, edited by L. Yaffe (Academic, New York, 1968), Vol. I, p. 169.

<sup>2</sup>N. T. Porile and N. Sugarman, *Phys. Rev.* **107**, 1422 (1957).

<sup>3</sup>N. Metropolis, R. Bivins, M. Storm, J. M. Miller, G. Friedlander, and A. Turkevich, *Phys. Rev.* **110**, 204 (1958).

<sup>4</sup>J. Benecke, T. T. Chou, C. N. Yang, and E. Yen, *Phys. Rev.* **188**, 2159 (1969).

<sup>5</sup>S. B. Kaufman, M. W. Weisfield, E. P. Steinberg, B. D. Wilkins, and D. Henderson, *Phys. Rev. C* **14**, 1121 (1976).

<sup>6</sup>S. K. Chang and N. Sugarman, *Phys. Rev. C* **9**, 1138 (1974).

<sup>7</sup>R. Wolfgang, E. W. Baker, A. A. Caretto, J. B. Cumming, G. Friedlander, and J. Hudis, *Phys. Rev.* **103**, 394 (1956).

<sup>8</sup>G. Friedlander, L. Friedman, B. Gordon, and L. Yaffe, *Phys. Rev.* **129**, 1809 (1963).

<sup>9</sup>E. M. Franz and G. Friedlander, *Nucl. Phys.* **76**, 123 (1966).

<sup>10</sup>C. J. Orth, B. J. Dropesky, R. A. Williams,

G. C. Giesler, and J. Hudis, *Phys. Rev. C* **18**, 1426 (1978).

<sup>11</sup>J. B. Cumming, P. E. Haustein, R. W. Stoenner, L. Mausner, and R. A. Naumann, *Phys. Rev. C* **10**, 739 (1974).

<sup>12</sup>J. B. Cumming, R. W. Stoenner, and P. E. Haustein, *Phys. Rev. C* **14**, 1554 (1976).

<sup>13</sup>J. B. Cumming, P. E. Haustein, T. J. Ruth, and G. J. Virtes, *Phys. Rev. C* **17**, 1632 (1978).

<sup>14</sup>W. Loveland, R. J. Otto, D. J. Morrissey, and G. T. Seaborg, *Phys. Rev. Lett.* **39**, 320 (1977); *Phys. Lett.* **69B**, 284 (1977).

<sup>15</sup>D. J. Morrissey, W. Loveland, and G. T. Seaborg, *Z. Phys.* **A289**, 123 (1978).

<sup>16</sup>N. T. Porile, G. D. Cole, and C. R. Rudy, *Phys. Rev. C* **19**, 2288 (1979).

<sup>17</sup>S. B. Kaufman, E. P. Steinberg, and G. W. Butler, *Phys. Rev. C* **20**, 2293 (1979).

<sup>18</sup>H. S. Pruys, R. Engfer, R. Hartmann, U. Sennhauser, H.-J. Pfeiffer, H. K. Walter, J. Morgenstern, A. Wyttenbach, E. Gadioli, and E. Gadioli-Erba, *Nucl. Phys.* **A316**, 365 (1979).

<sup>19</sup>H. P. Yule and A. Turkevich, *Phys. Rev.* **118**, 1591

- (1960).
- <sup>20</sup>J. B. Cumming, *Annu. Rev. Nucl. Sci.* **13**, 261 (1963).
- <sup>21</sup>R. Gunnink and J. B. Niday, UCRL Report No. 51061, 1972 (unpublished).
- <sup>22</sup>J. Hudis, T. Kirsten, R. W. Stoenner, and O. A. Schaeffer, *Phys. Rev. C* **1**, 2019 (1970).
- <sup>23</sup>E. Ross and K. Bächmann, *Radiochim. Acta* **21**, 13 (1974).
- <sup>24</sup>S. B. Kaufman, *Phys. Rev.* **129**, 1866 (1963).
- <sup>25</sup>E. Hagebø and H. Ravn, *J. Inorg. Nucl. Chem.* **31**, 897 (1969).
- <sup>26</sup>V. P. Crespo, J. M. Alexander, and E. K. Hyde, *Phys. Rev.* **131**, 1765 (1963).
- <sup>27</sup>R. G. Korteling and A. A. Caretto, *J. Inorg. Nucl. Chem.* **29**, 2863 (1967).
- <sup>28</sup>J. Hudis and S. Tanaka, *Phys. Rev.* **171**, 1297 (1968).
- <sup>29</sup>N. T. Porile, B. J. Drolesky, and R. A. Williams, *Phys. Rev. C* **18**, 2231 (1978).
- <sup>30</sup>J. R. Grover and A. A. Caretto, *Annu. Rev. Nucl. Sci.* **14**, 51 (1964).
- <sup>31</sup>Y.-W. Yu, A. A. Caretto, Jr., and L. B. Church, *Nucl. Phys.* **A152**, 295 (1970).
- <sup>32</sup>T. M. Kavanagh and R. E. Bell, *Can. J. Phys.* **39**, 1172 (1961).
- <sup>33</sup>M. V. Kantelo and J. J. Hogan, *Phys. Rev. C* **13**, 1095 (1976); *Phys. Rev. C* **14**, 64 (1976).
- <sup>34</sup>W. J. Treytl and A. A. Caretto, Jr., *Phys. Rev.* **146**, 836 (1966).
- <sup>35</sup>L. B. Church and A. A. Caretto, Jr., *Phys. Rev.* **178**, 1732 (1969).
- <sup>36</sup>W. J. Nieckarz, Jr. and A. A. Caretto, Jr., *Phys. Rev.* **178**, 1887 (1969).
- <sup>37</sup>S. B. Kaufman, E. P. Steinberg, and M. W. Weisfield, *Phys. Rev. C* **18**, 1349 (1978).
- <sup>38</sup>J. Hudis and S. Katcoff, *Phys. Rev.* **180**, 1122 (1969); *Phys. Rev. C* **13**, 1961 (1976).
- <sup>39</sup>G. Rudstam, *Z. Naturforsch.* **21a**, 1027 (1966).
- <sup>40</sup>R. Silberberg and C. H. Tsao, *Astrophys. J. Suppl. Ser. No. 220(I)*, **25**, 315 (1973); **25**, 335 (1973).
- <sup>41</sup>K. Chen, Z. Fraenkel, G. Friedlander, J. R. Grover, J. M. Miller, and Y. Shimamoto, *Phys. Rev.* **166**, 949 (1968).
- <sup>42</sup>G. D. Harp, K. Chen, G. Friedlander, Z. Fraenkel, and J. M. Miller, *Phys. Rev. C* **8**, 581 (1973).
- <sup>43</sup>J. N. Ginocchio, *Phys. Rev. C* **17**, 195 (1978).
- <sup>44</sup>I. Dostrovsky, Z. Fraenkel, and G. Friedlander, *Phys. Rev.* **116**, 683 (1959).
- <sup>45</sup>P. Kruger and N. Sugarman, *Phys. Rev.* **99**, 1459 (1955).
- <sup>46</sup>H. W. Bertini, *Phys. Rev. C* **6**, 631 (1972).
- <sup>47</sup>S. Kaufman, *Phys. Rev.* **126**, 1189 (1962).
- <sup>48</sup>S. Katcoff, H. R. Fickel, and A. Wyttbach, *Phys. Rev.* **166**, 1147 (1968).
- <sup>49</sup>J. R. Grover, *Phys. Rev.* **126**, 1540 (1962).
- <sup>50</sup>K. Beg and N. T. Porile, *Phys. Rev. C* **3**, 1631 (1971).
- <sup>51</sup>O. Scheidemann and N. T. Porile, *Phys. Rev. C* **14**, 1534 (1976).
- <sup>52</sup>S. B. Kaufman and M. W. Weisfield, *Phys. Rev. C* **11**, 1258 (1975).
- <sup>53</sup>S. Biswas and N. T. Porile, *Phys. Rev. C* **20**, 1467 (1979).
- <sup>54</sup>L. P. Remsberg and D. G. Perry, *Phys. Rev. Lett.* **35**, 361 (1975).
- <sup>55</sup>D. R. Fortney and N. T. Porile, *Phys. Lett.* **76B**, 553 (1978).
- <sup>56</sup>N. T. Porile, D. R. Fortney, S. Pandian, R. A. Johns, T. Kaiser, K. Wielgoz, T. S. K. Chang, N. Sugarman, J. A. Urbon, D. J. Henderson, S. B. Kaufman, and E. P. Steinberg, *Phys. Rev. Lett.* **43**, 918 (1979).